J Mater Sci (2009) 44:266–273
DOI 10.1007/s10853-008-3041-z

Effects of alumina in nonmetallic brake friction materials on friction performance

Vladimír Tomášek · Gabriela Kratošová · Rongping Yun · Yanli Fan · Yafei Lu

Received: 3 September 2007 / Accepted: 7 October 2008 / Published online: 10 November 2008

Abstract The effects of alumina (Al_2O_3) as an abrasive on brake friction performance and friction layers of nonmetallic brake friction materials were evaluated. Five experimental compositions containing from 0 to 14.6 vol% alumina were tested (Al_2O_3—0, 3.4, 5.6, 9.0, and 14.6 vol%). The experimental results indicated that alumina enhances friction coefficient and improves wear performance. The formation and development of friction layers were characterized using X-ray fluorescence spectrometry and scanning electron microscopy with energy dispersive X-ray analysis. Phenomena of baryte film and transferred iron-containing film formed on the friction surfaces were observed. Baryte films were detected on specimens containing from 0 to 5.6 vol% alumina. Iron-containing films were detected on surfaces of all alumina-containing specimens but not on the material without alumina. The role of abrasive in nonmetallic friction materials was studied in relation to formulation, friction performance, and friction surfaces.

V. Tomášek · G. Kratošová (✉)
Nanotechnology Centre, VSB-Technical University of Ostrava, 17. listopadu 15, 708 33 Ostrava-Poruba, Czech Republic
e-mail: gabriela.kratosova@vsb.cz

R. Yun · Y. Fan · Y. Lu
The Key Laboratory of Beijing City on Preparation and Processing of Novel Polymer Materials, Beijing University of Chemical Technology, Box 82, Beijing 100029, China

Introduction

Commercially available phenolic bound friction materials for automobile brakes can be classified into semi-metallic [1], nonasbestos organic (NAO) [2], and ceramic types [3]. NAO friction materials are one of the important types of modern friction materials used in brakes. They are composed mainly of organic and mineral fibers. Most NAO formulations contain fewer amounts of metal fibers (steel wool) and they are called as low-metallic NAO. Some other NAO formulations do not contain steel wool and they are designated as nonmetallic. Organic and mineral fibers (aramid pulp, oxidized polyacrylonitrile fiber, acrylic, cellulose, carbon, glass and slag fibers, wollastonite) are utilized in NAO formulations. The fillers used in NAO friction materials are abrasives, lubricants, space fillers, and functional fillers. The used abrasives including aluminum oxide (Al_2O_3), zircon ($ZrSiO_4$), zirconium oxide (ZrO_2), and silicon carbide (SiC) have higher Mohs hardness values of about 7–9. Graphite, coke, MoS_2, and Sb_2S_3 are often used as lubricants. Baryte ($BaSO_4$), calcium carbonate ($CaCO_3$), and calcium hydroxide ($Ca(OH)_2$) are utilized as space fillers to cut down the costs. Mica and vermiculite can be used as functional fillers to reduce the noise. Rubber or cashew-modified phenolics are currently used in NAO formulations as binders.

With the rapid development of automobile industry, the brakes require environmentally friendly friction materials with higher and stable friction coefficient μ and low wear rate, vibration, noise, and costs. To realize these requirements, combinatorial friction materials research (CFMR) has been developed. CFMR includes a combinatorial approach to screen raw materials [4–6], a Golden Section approach to optimize the friction performance [7], and investigations on the relationships among compositions,

friction layer characteristics, and friction performance [8]. Compared with the traditional classification of raw materials, the combinatorial approach classified the raw materials into group I and group II according to their wear resistance. Alumina, steel wool, aramid pulp, graphite, coke, MoS_2, powder rubbers, and phenolic resins have good wear resistance and they belong to group I [9]. Furthermore, the ingredients in group II can be classified into subgroups II-A and II-B according to their wear resistance by combinations of each ingredient of group I with a component of group II. For example, mixture of alumina (group I) with brass and copper chips (group II) is classified into group II-A, and this combination has good wear resistance. Next examples of group II-A are mixtures of graphite (group I) with brass, copper chips and potassium titanate whisker (group II) or combination of aramid pulp (group I) with potassium titanate whisker, wollastonite, vermiculite, baryte, mineral and slag fibers (group II).

By using the CFMR methodology, the NAO formulations without metals were designed with the ingredients of group I including alumina, aramid pulp, graphite, nitrile butadiene rubber (NBR), and phenolic and the ingredients of group II-A including mineral fiber with silica and alumina content, wollastonite, and baryte. The role of alumina in the NAO formulations and its effect on friction performance were studied.

Experimental

Raw materials

Raw materials used for our experiments are listed in Table 1. Alumina as a major component with the average size of 100 mesh was used as an abrasive, graphite as a lubricant, NBR and modified phenolic resin as a binder, and baryte as a filler. To reinforce friction composites, several fibrous materials were chosen: aramid pulp, wollastonite, and mineral fiber with the chemical compositions of SiO_2 (42.3 wt.%), Al_2O_3 (17.2 wt.%), CaO (15.4 wt.%), MgO (6.1 wt.%), Fe_2O_3 (4.0 wt.%), and C (5.7 wt.%).

Formulations and preparation of friction materials

Following volume fractions of Al_2O_3 were selected: 0, 3.4, 5.6, 9.0, and 14.6 vol%. Designed formulations of friction samples are listed in Table 2. The prepared friction composites were marked as Al-*x*, where *x* represents volume fraction of Al_2O_3 in the formulations. The volume of the phenolic binder fraction was kept constant, but the other components were proportionally decreased with the increase of alumina from 0 to 14.6 vol%. All raw materials were mixed using Electrolux EBR100 blender for 2 min. The mixture was pressed by a JFY60 device made by Jilin Wanda Mechanical Co, Ltd. at a temperature of 165 °C, pressure of 25 MPa, and duration of 6 min. The friction materials were post-treated at 120 °C for 60 min, at 150 °C for 60 min, and at 180 °C for 120 min.

Tests of friction performance

Friction performance of studied materials was tested based on China National Standard GB5763-1998 (brake linings for automobiles) by a JF151 friction tester (Jinlin Wanda Mechanical Co. Ltd, Fig. 1) with a constant speed of 7.54 m/s and constant load of 0.98 MPa. The disk made of cast iron (grade HT250 with Brinell hardness in the range

Table 2 Relative content (in vol%) of raw materials in the designed samples used

Raw materials	Samples				
	Al-0	Al-3.4	Al-5.6	Al-9	Al-14.6
Twaron	23.6	22.55	21.87	20.82	19.09
Mineral fiber	9.0	8.60	8.34	7.94	7.28
Wollastonite	2.2	2.10	2.04	1.94	1.78
Baryte	23.6	22.55	21.87	20.82	19.09
Graphite	9.0	8.60	8.34	7.94	7.28
NBR	9.0	8.60	8.34	7.94	7.28
Phenolic	23.6	23.6	23.6	23.6	23.6
Al_2O_3	0	3.4	5.6	9.0	14.6

Table 1 Raw materials used for experiments

Raw materials	Trademark	Manufacturer
Aramid pulp	Twaron 1099	Teijin Twaron GmbH
Mineral fiber	4025Y	Bejing Hengnian Tech Trade Co. Ltd
Wollastonite	Needle Type	Astron Chemical (Yingkou) Co. Ltd
Graphite	Mg-20	Changzhou Wujin Special Fibers Co. Ltd
Baryte ($BaSO_4$)	80%	Zaoyang Wulian Co. Ltd
Alumina (Al_2O_3)	B211-G	Zibao China Aluminum Industry Group
NBR powder	P650	Guangzhou Asia Rubber Co. Ltd
Phenolic resin	6818	Jinan Shengquan Hepworth Chem Co. Ltd

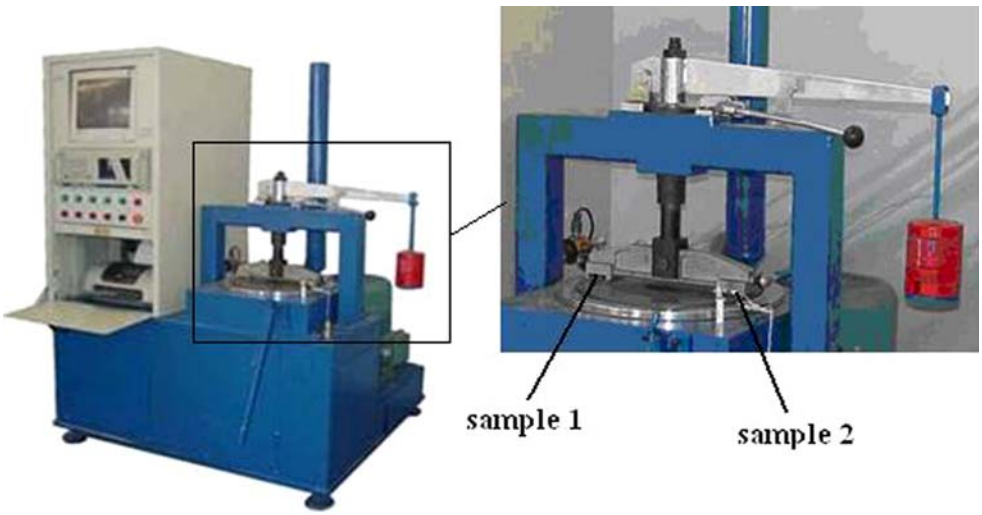

Fig. 1 JF151 friction tester

180–220) was used as a rotor and a friction composite sample of size 2.5 × 2.5 × 0.6 cm^3 as a stator. Two same samples were tested in parallel. The data of both friction coefficient measured during heating process (fade, μ_f) and volume wear rate (V) were obtained after 5,000 rotations of the disk at each temperature of 100, 150, 200, 250, 300, and 350 °C. Fade is a temporary reduction of the braking effectiveness due to loss of friction between the braking surfaces, resulting from heat. V was calculated by the formula $V = \frac{1}{2\pi R} \times \frac{A}{n} \times \frac{d_1 - d_2}{f_m}$ in cm^3/(N m), where R is the distance between the specimen center and the center of rotating disk (0.15 m), n is the number of rotations (5,000), A is the specimen area (2.5 × 2.5 cm^2), d_1 is the average thickness of a specimen before experiment (cm), d_2 is the average thickness of a specimen after experiment (cm), and f_m is the average force of sliding friction (N). The friction coefficient data measured during cooling process (recovery, μ_r) were obtained after 2,000 rotations of the disk at each temperature of 300, 250, 200, 150, and 100 °C. Once the brake lining cools, it should repeatedly recover its original friction coefficient—this is termed as recovery.

Evaluation of friction surfaces

Friction surfaces of samples after friction tests were examined using scanning electron microscope (SEM) with energy dispersive X-ray analyzer (EDX). SEM micrographs were obtained with Philips Scanning Electron Microscope XL 30 using backscattered electrons at an operating voltage of 25 kV. Electron microprobe analyses (EMA) were performed in points or areas marked on the micrographs. For the correct quantitative analysis, it is necessary to have polished samples; however, to study friction layers it is not possible to perform this sample treatment. Therefore, analyses results are not presented in quantitative form, but only identified phases and other major elements are mentioned.

Differences between chemical composition of friction surfaces after friction tests and original material (bulk material) were examined using EMA and X-ray fluorescence spectrometry (XRF). EMA was performed at 50× magnification; it means that an area of approximately 2.5 × 2.0 mm^2 was analyzed in one measurement, and the depth of analyzed sample is approximately 1–2 μm. Three different areas on each friction surface (friction layer—FL) and three on the backside of every sample (bulk material—BM) were analyzed. Similar measurements were made using XRF method (X-ray energy-dispersive spectrometer SPECTRO X-LAB). Area in diameter of approximately 10 mm was analyzed in one measurement. The depth of analyzed material estimation is difficult because of its heterogeneity but it is much higher than in the case of EMA. The depth of analyzed material is approximately 1 mm. To express the changes of selected elements concentration during friction process, the ratio of elements concentration in friction layer to their concentration in original material (FL/BM) was calculated. Dependences of FL/BM on alumina volume concentration in original friction materials are presented graphically.

Results and discussion

Effects of alumina on friction performance

The effects of alumina on μ_f and μ_r are shown in Fig. 2a and b. The values of μ_f and μ_r are enhanced by the addition of alumina into the friction formulations. When the content of alumina is 0 (Al-0) and the testing temperature is 350 °C, μ_f is low (=0.158). However, with the increasing

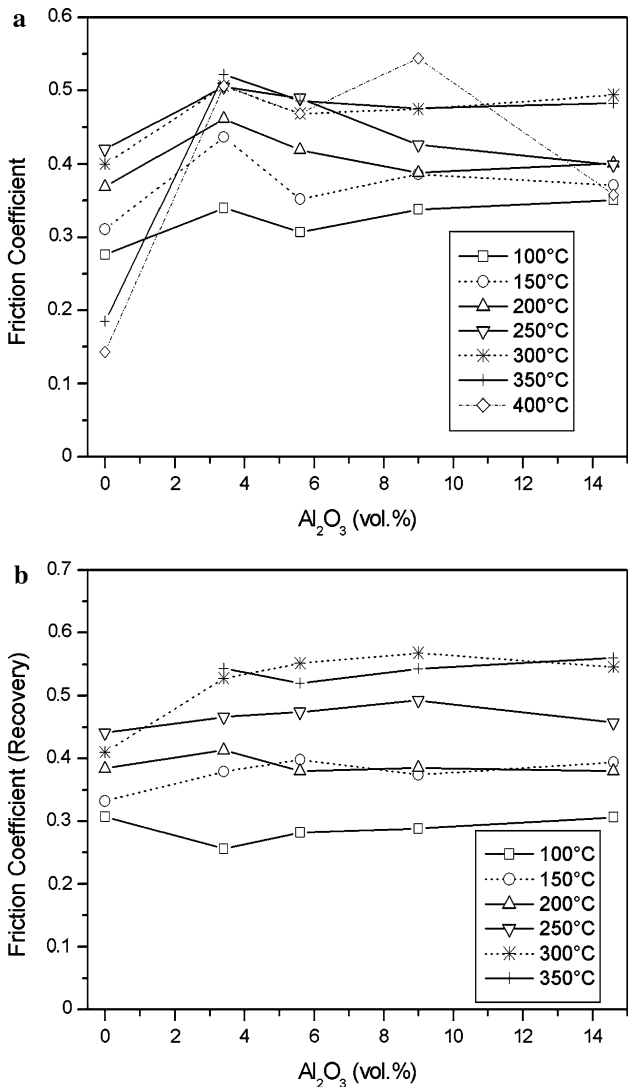

Fig. 2 Alumina and temperature effects on **a** μ_f and **b** μ_r

alumina content, the values of μ_f of the friction materials increase.

To evaluate quantitatively the complex and nonlinear relationship among friction coefficients μ_f and μ_r composition, and temperature, following formulae based on fuzzy comprehensive evaluation method were utilized [10]:

$$\Delta\mu^* = \frac{\sum_{i=1}^{5} N_i \times \frac{|\mu_f-\mu_r|_{max}-|\mu_f-\mu_r|_i}{|\mu_f-\mu_r|_{max}-|\mu_f-\mu_r|_{min}} + N_6}{n} \quad (1)$$

$$N = \begin{Bmatrix} 1.00, & \mu \in [0.40, 0.50] \\ 0.75, & \mu \in [(0.35, 0.40) \cup (0.50, 0.55)] \\ 0.50, & \mu \in [(0.30, 0.35) \cup (0.55, 0.60)] \\ 0.25, & \mu \in [(0.25, 0.30) \cup (0.60, 0.70)] \\ 0.00, & \mu \in [(0.00, 0.25) \cup (0.7, X)] \end{Bmatrix} \quad (2)$$

where $\Delta\mu^*$ is defined as a friction stability; $i = 100$, 150, 200, 250, and 300 °C, respectively, N_i is the weight at i temperature, and N_6 is the weight at 350 °C and can be directly obtained from Eq. 2. The ranges of both μ_f and μ_r at a certain temperature allowed by GB5763-1998 are 0.25–0.65 at 100 °C, 0.25–0.70 at 150 °C, 0.25–0.70 at 200 °C, 0.25–0.70 at 250 °C, 0.25–0.70 at 300 °C, and 0.20–0.70 at 350 °C, respectively. If any one of the μ_f and μ_r values are out of the range, then $\Delta\mu^* < 0$. It means the friction material does not meet the requirement of GB5763–1998 testing procedure and cannot be used as brake pads to automobiles. The friction testing results show that μ_f (at temperature 350 °C) of Al-0 sample is equal to 0.185, so $\Delta\mu^* < 0$. Within the allowed region, the larger the $\Delta\mu^*$, the best the friction stability.

The evaluated friction stability is shown in Table 3. Sample Al-5.6 has the best friction stability among the formulations and this means little effect of friction temperature on friction coefficient.

The effects of alumina on wear in examined samples are shown in Fig. 3. Sample Al-0 shows its wear rate < 0 (negative wear) at 250 °C. It may be caused by either gas release or thermal expansion of friction materials. The wear rate of friction materials with alumina is a little larger than that without alumina. However, alumina can improve negative wear performance.

Table 3 The evaluated results for both friction stability and comprehensive wear rate

	Al-0	Al-3.4	Al-5.6	Al-9.0	Al-14.6
$\Delta\mu^*$	<0	0.45	0.50	0.39	0.44
M_A	>1	0.22	0.14	0.19	0.29

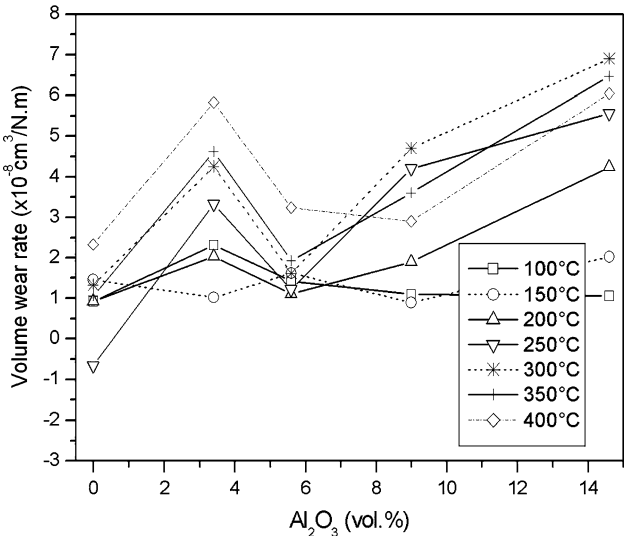

Fig. 3 Alumina and temperature effects on wear

To normalize and quantitatively evaluate nonlinear wear as a function of alumina concentration at different temperatures, following formula was utilized [10]:

$$M_{\mathrm{A}} = \frac{\sum_{j=1}^{6} \left(\frac{\omega(T)}{S(T)}\right)_j}{n} \quad (3)$$

where M_{A} is defined as the comprehensive wear rate, T is the temperature; $j = 100$, 150, 200, 250, 300, and 350 °C, respectively, and $\omega(T_j)$ and $S(T_j)$ are the determined wear value and the maximum allowed by GB5763-1998 at j temperature, respectively. The $S(T_j)$ values are $S(100\ ^\circ\mathrm{C}) = 0.50$, $S(150\ ^\circ\mathrm{C}) = 0.70$, $S(200\ ^\circ\mathrm{C}) = 1.00$, $S(250\ ^\circ\mathrm{C}) = 1.50$, $S(300\ ^\circ\mathrm{C}) = 2.50$, and $S(350\ ^\circ\mathrm{C}) = 3.50$. If any one of the $\omega(T_j)$ values < 0 (negative wear) and/or >1 (over the allowed value), $M_{\underline{a}} > 1$. It means the friction material cannot be used as brake pads to automobiles. So within the region of 0–1, the smaller the M_{A}, the best the comprehensive wear rate.

The evaluated wear rates are shown in Table 3. Sample of Al-5.6 has the best wear rate. Comprehensively, Al-5.6 shows the maximum $\Delta\mu^*$ (best friction stability) and smallest M_{A} (best wear), so this sample exhibits the best comprehensive friction performance among the tested formulations. In general, alumina as an abrasive in nonmetallic friction materials plays an excellent role in enhancing the friction coefficient and improve wear, but its amount needs to be optimized.

Analysis of friction surfaces and relationships between friction layers and friction performance

Friction layers evaluation is important for the understanding of correlation of the compositions with friction performance. The basic images related to the structure of friction layers are clear. The friction layers composed of primary and secondary contact plateaus were characterized by Eriksson et al. [11, 12]. The matter transfer direction of debris to the surfaces of either disk or friction materials is dependent upon the abrasion or adhesion [13]. The formation and destruction mechanisms of friction layers were studied and proposed by Österle et al. [14–16], Cho et al. [17], and Ostermayer et al. [18, 19].

To understand why sample Al-5.6 has good friction performance, the friction layers of NAO friction materials containing alumina were analyzed, as shown in Figs. 4, 5, 6 and 7.

The friction layer of Al-0 has been investigated in detail in our previous work [8]. This transferred iron-containing film from the cast iron disk and baryte film formed on the Al-0 friction surface were observed.

The characteristics of friction layer of Al-3.4 are shown in Fig. 4. Both transferred iron-containing film (Fig. 4a, point 1) and baryte film (Fig. 4b, area 2) were identified on the friction layers of composites with alumina. Iron transfer from the cast iron disk to the surface of nonmetallic friction materials was caused by alumina because the hardness of

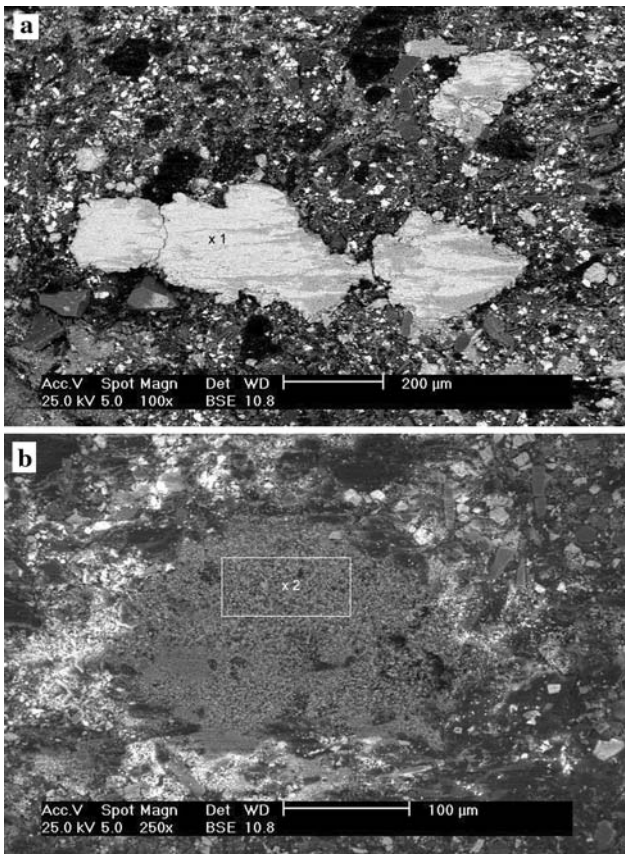

Fig. 4 SEM micrograph of friction surface for Al_2O_3-3.4 vol% sample, tested at 350 °C, BSE, **a** magnification 100×, transferred iron-containing film—point 1, **b** magnification 250×, analyzed area—baryte film, other identified elements: Al, Si, Ca, Fe, and Mg

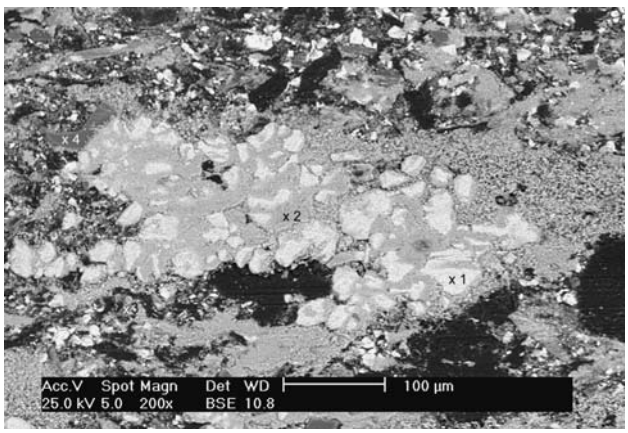

Fig. 5 SEM micrograph of friction surface for Al_2O_3-5.6 vol% sample, tested at 350 °C, BSE, magnification 200×; point 1—Fe, point 2 is a mixture of baryte and debris formed by other ingredients (Si, Mg, and Ca)

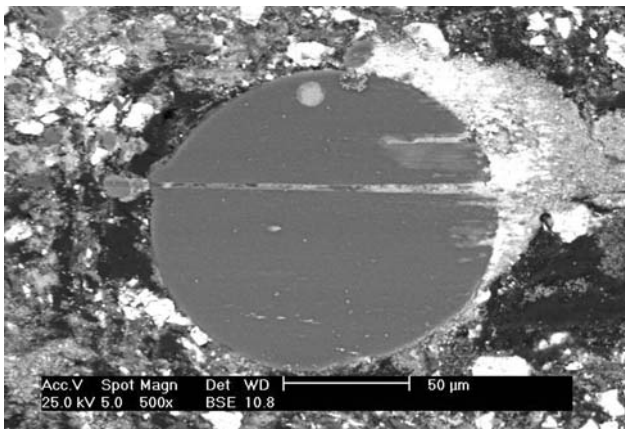

Fig. 6 SEM micrograph of friction surface for Al_2O_3-9.0 vol% sample, tested at 350 °C, BSE, magnification 500×, growing edge of debris around mineral fiber on the surface

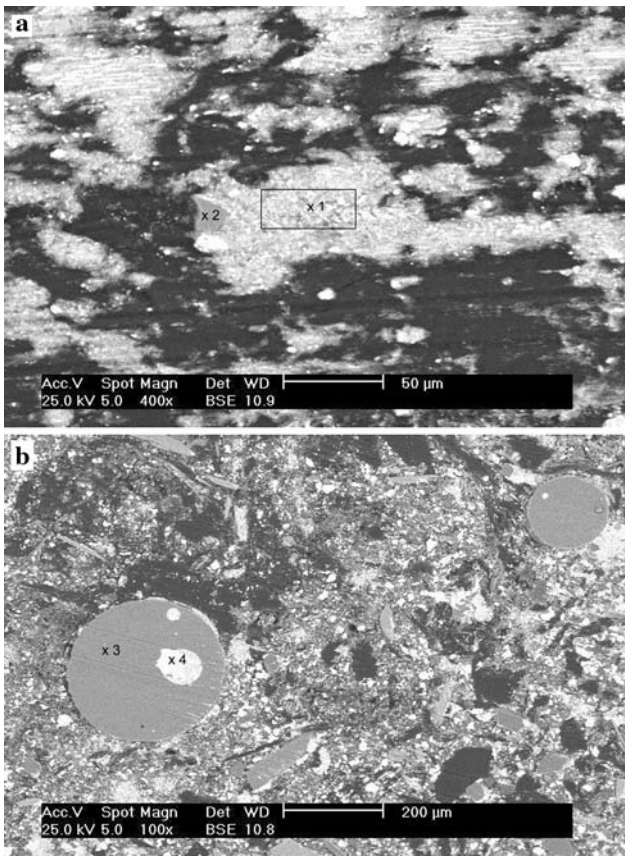

Fig. 7 SEM micrograph of friction surface for Al_2O_3—14.6 vol% sample, tested at 350 °C, BSE, **a** magnification 400×, area 1—transferred iron-containing film, other identified elements Al, Ba, S, Ca, O, Si; point 2—mineral fiber (Ca, Si, Al, Mg, O); **b** magnification 400×, point 3—mineral fiber (Al, Si, O), point 4—Fe

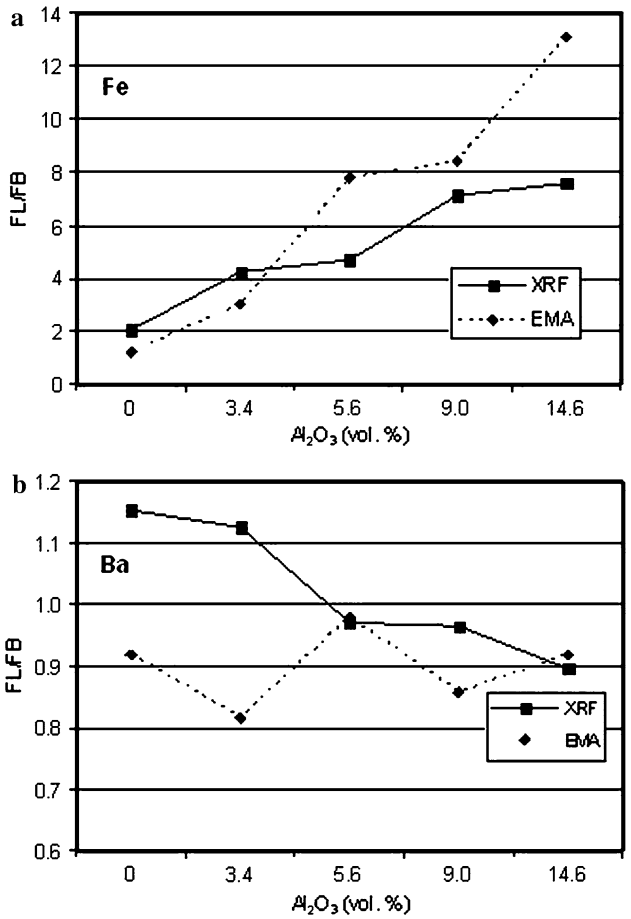

Fig. 8 Ratio between Fe (**a**) and Ba (**b**) concentrations in friction layer and bulk material (FL/BM) determined by XRF and EMA methods depending on alumina concentration in original material

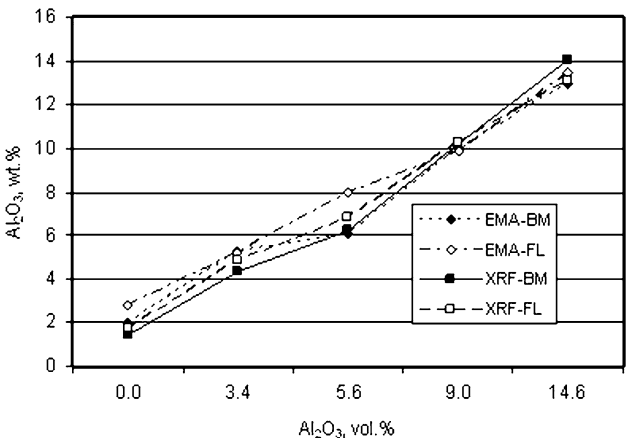

Fig. 9 Concentration of Al_2O_3 in friction layer (FL) and bulk material (BM) determined by XRF and EMA methods in dependence to vol% of Al_2O_3 in original material

the abrasive is larger than that of cast iron [13]. Transferred iron-containing film is more on the friction surface of Al-5.6, but the baryte film is less (Fig. 5).

The role of mineral fiber in the formation of primary and secondary contact plateaus, like in the case of steel wool [13], was observed, as shown in Figs. 6 and 7.

Table 4 Relationships among formulations, friction performance, and friction surfaces

Samples	Friction performance	Main friction layers characteristics
Al-0	Lower μ and good wear	Baryte film
Al-3.4	Higher stable μ and poor wear	Baryte film and transferred iron-containing film
Al-5.6	Higher stable μ and good wear	Less baryte film and transferred iron-containing film
Al-9.0, Al-14.6	Higher stable μ and poor wear	More transferred iron-containing film

Iron-containing traces and grooves parallel to the disk rotation direction appeared on the friction surface of Al-9 (Fig. 6). More transferred iron-containing film was found on the friction surface of Al-14.6, as shown in Fig. 7. It is reasonable because the amount of alumina increased.

Changes of friction surface chemical composition in comparison to original material

The modification of friction surface chemical composition during friction tests were evaluated by the ratio of selected elements concentration in friction layer to their concentration in bulk material (FL/BM). The concentrations were determined using EMA and XRF methods. In spite of the very thin friction layers produced by used test procedure, enrichment of these layers by Fe are clear. Iron concentration in friction layers markedly increases with increasing Al_2O_3 concentration in original material as shown in Fig. 8a. Considering a very low concentration of Fe in original material from natural minerals in composition (about 0.3 wt. %), the increasing Fe concentration in friction surfaces can be caused only by transfer from cast iron disk. The Fe enrichment of the friction layer measured by EMA method is a little higher than when determined by XRF method. It is probably caused by the thickness of the analyzed material. EMA method analyzes a much thinner layer than XRF method and enrichment of this very thin layer is higher.

Changes of Ba concentrations in the friction layers after friction tests are documented in Fig. 8b. The concentration of Ba measured by XRF method slightly decreases with increasing Al_2O_3 concentration in original friction material. Other elements like S, Mg, and Si show similar dependences. Al-0 has more baryte film but less transferred iron-containing film and conversely Al-14.6 has more transferred iron-containing film but less baryte film. Changes of Ba concentration in surface layers using EMA method are not evident. Inhomogeneities of the samples cause higher fluctuation of obtained results.

Concentrations of Al_2O_3 obtained using both EMA and XRF methods are very similar (Fig. 9). No significant changes in alumina concentrations on friction layers in comparison to original material were observed.

Relationships among formulations, friction performance, and friction surfaces

The relationships among formulations, friction performance, and friction surfaces are summarized in Table 4. It was found that if compositions in the bulk are similar to the surface composition of sample Al-5.6, stable μ and good wear can be obtained. Alumina plays a crucial role in affecting friction layers. Without alumina, a baryte film was formed. With the higher alumina content, the formation of baryte film declined and transferred iron-containing film increased. The transition occurred near 5.6 vol% of alumina.

Conclusions

The effects of alumina content on friction performance were comprehensively evaluated. Alumina as an abrasive plays a key role in enhancing the μ values and in eliminating the negative wear rate of the nonmetallic friction materials. From the evaluated results of friction stability and wear, Al-5.6 formulation is the best one. Analyzing friction surfaces of tested samples, baryte film, iron traces, grooves, and transferred iron-containing film were observed. Friction layers are markedly enriched by iron, and the iron-containing film formation with alumina content increases. A new friction mechanism related to the formation and destruction of two types of films was proposed to explain the relationships among the compositions, friction layer, and friction performance.

Acknowledgements The authors acknowledge National Natural Science Foundation of China (50673012), Twaron Research Fund (Teijin Twaron GmbH, Germany, 2007), Programs of International Cooperation funded by Ministry of Education, Youth and Sports of Czech Republic 1P05ME741, and Ministry of Education, Youth and Sports of the Czech Republic (MSM 6198910016) for their financial supports.

References

1. Lu Y, Tang CF, Zhao Y, Wright MA (2004) J Reinf Plast Compos 23:1537

2. Lu Y (2003) J Mater Sci 38:1081. doi:10.1023/A:1022362217043
3. Han L, Huang L, Zhang J, Lu Y (2006) Compos Sci Tech 66:2895
4. Lu Y (2002) Polym Compos 23:814
5. Tang CF, Lu Y (2004) J Reinf Plast Compos 23:51
6. Lu Y (2006) Compos Sci Tech 66:591
7. Lu Y, Tang CF, Wright MA (2002) J Appl Polym Sci 84:2498
8. Ma Y, Martynková GS, Valášková M, Matějka V, Lu Y (2008) Tribol Int 41(3):166
9. Zhao Y, Lu Y, Wright MA (2006) Mater Design 27:833
10. Fan Y, Han L, Lu Y (2006) Non-metall Mines 29(5):63 (in Chinese)
11. Eriksson M, Bergman F, Jacobson S (2002) Wear 252:26
12. Eriksson M, Bergman F, Jacobson S (1999) Wear 232:163
13. Landolt D, Mischler S, Stemp M, Barril S (2004) Wear 256:517
14. Österle W, Urban I (2004) Wear 257:215
15. Österle W, Griepentrog M, Th Gross, Urban I (2001) Wear 251:1469
16. Österle W, Kloß H, Urban I, Dmitriev AI (2007) Wear 263:1189
17. Cho MH, Cho KH, Kim SJ, Kim DH, Jang H (2005) Tribb Lett 20(2):101
18. Ostermeyer GP, Muller M (2006) Trib Int 39:370
19. Muller M, Ostermeyer GP (2007) Trib Int 40:942